J|A|C|S ARTICLES

Published on Web 04/26/2010

Room-Temperature Synthesis Leading to Nanocrystalline $Ag_2V_4O_{11}$

Frédéric Sauvage,[†] Vincent Bodenez,[‡] Jean-Marie Tarascon,[‡] and Kenneth R. Poeppelmeier*,[†]

Department of Chemistry, Northwestern University, Evanston, Illinois 60208-3113, and LRCS, UMR CNRS 6007, Université de Picardie Jules Verne, 33 Rue St.-Leu, 80039 Cedex, France

Received February 3, 2010; E-mail: krp@northwestern.edu

Abstract: This work highlights a room-temperature composition study of the $Ag_2O/V_2O_5/HF_{(aq)}$ ternary system, leading to the precipitation of either various silver vanadates having Ag/V ratios from 1/2 to 3/1 or the new silver vanadium oxyfluoride compounds $Ag_4V_2O_6F_2$ and $Ag_3VO_2F_4$, and a synthetic procedure that affords nanocrystalline $Ag_2V_4O_{11}$ (SVO) at room temperature. The as-precipitated SVO particles exhibit an acicular morphology, 10−15 × 50−200 nm in size, and present a peculiar reactivity vs lithium notably through a Ag^+/Li^+ displacement reaction that progresses in a reversible fashion. This step forward thus enables the reversible and simultaneous combination of two active redox processes (silver and vanadium), providing a significant enhancement in the cathode gravimetric capacity of 320 mAh/g at C rate and more than 250 mAh/g at 5C.

Introduction

The need for energy storage gave rise to the lithium-ion battery, while the effort given to the synthesis of nanomaterials has challenged preconceived criteria in the search for better performing insertion materials for Li^+ storage. One of the most important challenges was to design a structure for a new electrode material that combines both high electronic conductivity and high lithium mobility. Although these two characteristics are in principle still required, their limit has been reached given that an insulating cathode material, namely, the olivine structure $LiFePO_4$, can be successfully used as positive electrode in Li-ion batteries, despite a very low intrinsic electronic conductivity of ca. 10^{-9} S/cm and a lower ionic conductivity.[1−3] Recent studies of other insulating materials has led to similar results in particular with the isostructural, higher power, $LiMnPO_4$, for which 156 mAh/g has been reached despite $\sigma_{(e-)} \approx 10^{-14}$ S/cm[4−7] or 100−130 mAh/g for silicates.[8−11] In these cases, the poor carrier transport has been overcome by the reduction of the particle's size while orienting the growth of the crystals to reduce the e^-/Li^+ motion length from the core to the shell of the particle. As a corollary, the electrochemical reactivity becomes dominated by the particle's surface with consequences such as the onset of unusual phenomena originating from surface defects or band bending. This leads, in some cases, to a significant alteration of the electrochemical properties with respect to well-established bulk phenomena.[12−15] Interest in nanoscale materials has triggered soft chemistry methods, including hydrothermal/solvothermal approaches as well as sol−gel and more recently ionothermal strategies using ionic liquids as the solvent[16−19] to accurately control nucleation vs growth processes and hence manipulate the morphology and size of the desired compound. These soft methods, in contrast to the more classical ceramic approach, are less energetically demanding.[20]

[†] Northwestern University.
[‡] Université de Picardie Jules Verne.

(1) Padhi, A. K.; Nanjundaswamy, K. S.; Goodenough, J. B. *J. Electrochem. Soc.* **1997**, *144*, 1188–1194.
(2) Delacourt, C.; Wurm, C.; Laffont, L.; Leriche, J.-B.; Masquelier, C. *Solid State Ionics* **2006**, *177*, 333–341.
(3) Sauvage, F.; Baudrin, E.; Gengembre, L.; Tarascon, J.-M. *Solid State Ionics* **2005**, *176*, 1869–1876.
(4) Drezen, T.; Kwon, N.-H.; Bowen, P.; Teerlinck, I.; Isono, M.; Exnar, I. *J. Power Sources* **2007**, *174*, 949–953.
(5) Delacourt, C.; Poizot, P.; Morcrette, M.; Tarascon, J.-M.; Masquelier, C. *Chem. Mater.* **2004**, *16*, 93–99.
(6) Wang, D.; Buqa, H.; Crouzet, M.; Deghenghi, G.; Drezen, T.; Exnar, I.; Kwon, N.-H.; Miners, J. H.; Poletto, L.; Graetzel, M. *J. Power Sources* **2009**, *189*, 624–628.
(7) Martha, S. K.; Markovsky, B.; Grinblat, J.; Gofer, Y.; Haik, O.; Zinigrad, E.; Aurbach, D.; Drezen, T.; Wang, D.; Deghenghi, G.; Exnar, I. *J. Electrochem. Soc.* **2009**, *156*, A541–A552.
(8) Prakash, A. S.; Rozier, P.; Dupont, L.; Vezin, H.; Sauvage, F.; Tarascon, J.-M. *Chem. Mater.* **2006**, *18*, 407–412.
(9) Dominko, R.; Conte, D. E.; Hanzel, D.; Gaberscek, M.; Jamnik, J. *J. Power Sources* **2008**, *178*, 842–847.
(10) Dominko, R. *J. Power Sources* **2008**, *184*, 462–468.
(11) Nadherna, N.; Dominko, R.; Hanzel, D.; Reiter, J.; Gaberscek, M. *J. Electrochem. Soc.* **2009**, *156*, A619–626.
(12) Meethong, N.; Kao, Y. H.; Tang, M.; Huang, H.-Y.; Craig Carter, W.; Chiang, Y.-M. *Chem. Mater.* **2008**, *20*, 6189–6198.
(13) Larcher, D.; Bonnin, D.; Cortes, R.; Rivals, I.; Personnaz, L.; Tarascon, J.-M. *J. Electrochem. Soc.* **2003**, *150*, A1643–A1650.
(14) Wagemaker, M.; Borghols, W. J. H.; Mulder, F. M. *J. Am. Chem. Soc.* **2007**, *129*, 4323–4327.
(15) Baudrin, E.; Cassaignon, S.; Koelsch, M.; Jolivet, J. P.; Dupont, L.; Tarascon, J.-M. *Electrochem. Commun.* **2007**, *9*, 337–342.
(16) Parnham, E. R.; Morris, R. E. *Acc. Chem. Res.* **2007**, *40*, 1005.
(17) Lin, Z.-J.; Li, Y.; Slawin, A. M. Z.; Morris, R. E. *Dalton Trans.* **2008**, 3989.
(18) Recham, N.; Laffont, L.; Armand, M.; Tarascon, J.-M. *Electrochem. Solid State Lett.* **2009**, *12*, A39.
(19) Recham, N.; Dupont, L.; Courty, M.; Djellab, K.; Larcher, D.; Armand, M.; Tarascon, J.-M. *Chem. Mater.* **2009**, *21* (6), 1096–1107.
(20) Recham, N.; Armand, M.; Tarascon, J.-M. *C. R. Chim.* **2010**, *13*, 106–116.

10.1021/ja1009713

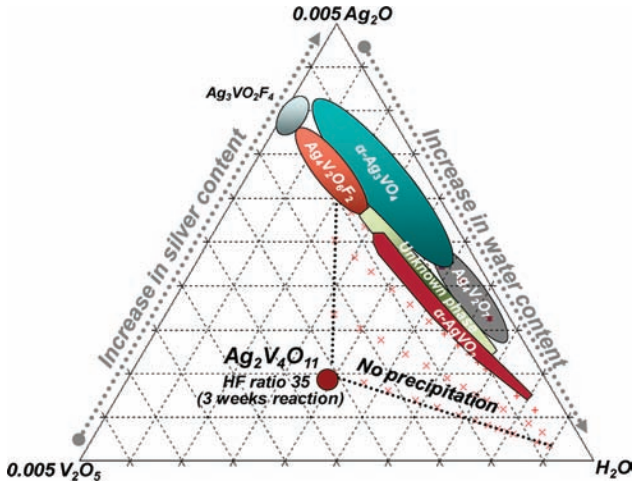

Figure 1. Schematic of the ternary diagram $Ag_2O/V_2O_5/H_2O$ using a 30 equivalent ratio of HF as mineralizer.

As an extension of soft chemistry methods, we have reported recently a strategy to precipitate at room temperature a promising silver dense oxyfluoride compound, $Ag_4V_2O_6F_2$ (SVOF), using an appropriate ratio of Ag_2O and V_2O_5 in $HF_{(aq)}$.[21] In that study, it was shown that the HF concentration plays a major role in the stoichiometry of the final product, and we have used such a finding to synthesize a new silver dense vanadium oxyfluoride compound, $Ag_3VO_2F_4$, adopting the cryolite-type structure. A peculiar aspect of silver-based phases, in particular for the Ag−V−O and Ag−V−O−F systems, lies in their particular reactivity toward lithium by a displacement reaction. The reduction of silver ion combined with that of vanadium (V^{5+}) offers greater gravimetric/volumetric capacity while maintaining the material electro-activity in the stability potential window of the electrolyte. Owing to the lack of reversibility of the silver displacement reaction, the benefit of such a cooperative mechanism, however, is restricted to primary lithium batteries. This work is a continuation in part of our ongoing exploration to stabilize new oxide-fluoride phases within the ternary system $Ag_2O-V_2O_5-H_2O$ when reacting in HF-resistant FEP-type pouches. In particular, on the basis of the ternary diagram experimentally obtained, we present a methodology that affords the precipitation of $Ag_2V_4O_{11}$ (SVO) under room-temperature control; SVO is of special interest as a cathode material for medical primary lithium batteries.[22] Interestingly, the nanocrystalline particles exhibit a reversible silver displacement reaction that when combined with the vanadium redox couple affords a gravimetric capacity exceeding 300 mAh/g with good rate capability.

Results and Discussion

We first constrained the investigation of this ternary system by maintaining the HF ratio to 30. Under such conditions several stability regions exist (as shown in Figure 1) where various silver vanadium-based oxides could be precipitated. At the center of a given region the product recovered was always well-crystallized and single-phase (see Supporting Information, Figure S1), while a mixture of two phases was observed near the border between two domains. The cell parameters for the different materials are reported in Table 1.

Table 1. Lattice Cell Parameters Refined for the Different Room-Temperature Precipitated Phases Synthesized in the Ternary System $Ag_2O-V_2O_5-H_2O$ Using a HF Ratio of 30 as a Mineralizer

	a (Å)	*b* (Å)	*c* (Å)	*β* (deg)	space group
α-$AgVO_3$	10.445(7)	9.901(5)	5.523(3)	99.68(3)	*C*2/*c*
$Ag_4V_2O_7$	18.821(6)	10.880(6)	13.928(9)	90	*Pbca*
α-Ag_3VO_4	10.311(9)	4.998(3)	10.259(7)	116.01(2)	*C*2/*c*
$Ag_4V_2O_6F_2$	5.601(1)	10.551(2)	12.511(3)	90.36(3)	$P2_1/n$
$Ag_3VO_2F_4$	5.854(6)	5.812(4)	8.504(7)	91.22(3)	$P2_1/n$

The silver content within the final product is mainly controlled by the HF and the precursor concentrations. Note it is also driven by the silver to vanadium precursor ratio to a lesser extent. This ratio can vary drastically from Ag/V = 3 for $Ag_3VO_2F_4$ and α-Ag_3VO_4 to Ag/V = 2 for $Ag_4V_2O_6F_2$ and $Ag_4V_2O_7$, and Ag/V = 1 giving α-$AgVO_3$. This result is in line with the observations realized by Shivahare, who reported a relationship between the nitric acid concentration and the Ag_2O/V_2O_5 ratio in the room-temperature-formed precipitate.[23] In addition, an unknown phase with similar Ag/V = 1 ratio, as deduced from EDX analyses, has been isolated. Its domain of existence is somewhat limited in the diagram. There is a large domain of Ag to V ratio and HF concentration where there is an absence of any solid (see Figure 1). Moreover, similar to the influence of the silver content, we also note that the HF concentration controls the fluorine to oxygen ratio in the final product. It can vary from 2 to 1/3 or 0 when reducing the acid quantity. Increasing the concentration of the reacting species enhanced the formation kinetics of the precipitated phases.

Note also that missing from this ternary diagram are silver vanadates with a Ag/V ratio less than 1; in particular the phase $Ag_2V_4O_{11}$ (SVO), which is of particular concern for medical lithium battery applications, is absent. To prepare SVO under room-temperature conditions, we adapted the aforementioned conditions by increasing the HF ratio to 35 and increasing the reaction time in order to compensate for the slow dissolution of V_2O_5. After three weeks reaction at room temperature, we successfully achieved single-phased nanocrystalline SVO using a Ag_2O/V_2O_5 ratio of 1/1.7. XRD investigations during the course of the reaction showed that the dissolution of the vanadium oxide governs the precipitation of SVO and that no crystalline intermediate phases were formed. All recorded X-ray reflections are indexed according to SVO reported structure (Figure 2). The noticeable broadness of the reflections demonstrates the nanocrystalline state, which is confirmed by the transmission electron micrograph shown in the inset. The morphology of the particles exhibits an acicular shape that is 10−15 nm wide and 50−200 nm in length. The nitrogen sorption experiment features a type IV adsorption/desorption isotherm revealing mesopores leading to a BET surface area of 28 m^2/g. This is greater than the 5 m^2/g determined for the nanoparticles prepared under hydrothermal conditions or <1 m^2/g for the particles prepared by the traditional solid-state method.[24]

The electrochemical properties of these nanocrystalline particles have been tested with respect to lithium metal. A typical galvanostatic signature is reported in Figure 3; here, we have

(21) Albrecht, T. A.; Sauvage, F.; Bodenez, V.; Tarascon, J.-M.; Poeppelmeier, K. R. *Chem. Mater.* **2009**, *13*, 3017–3020.
(22) Takeuchi, E. S.; Thiebolt, W. C., III. *J. Electrochem. Soc.* **1988**, *135* (11), 2691.
(23) Shivahare, G. C. *J. Inorg. Nucl. Chem.* **1966**, *28*, 657–658.
(24) Sauvage, F.; Bodenez, V.; Vezin, H.; Morcrette, M.; Tarascon, J.-M.; Poeppelmeier, K. R. *J. Power Sources* **2010**, *182* (2), 1195–1201.

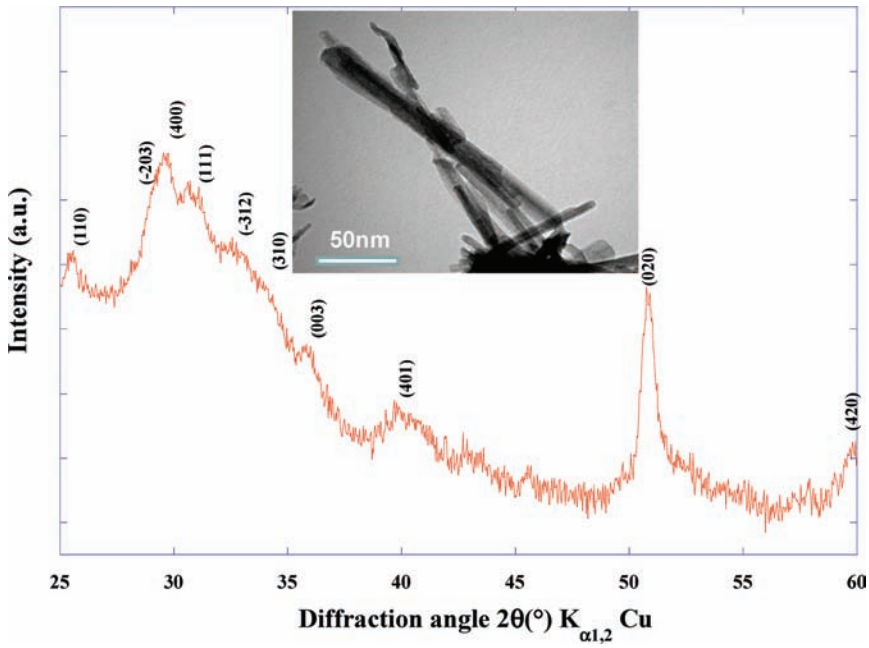

Figure 2. X-ray diffraction pattern of $Ag_2V_4O_{11}$ synthesized at room temperature (note the glue used for measurement is responsible for the background contribution). TEM of the particles is shown in the inset.

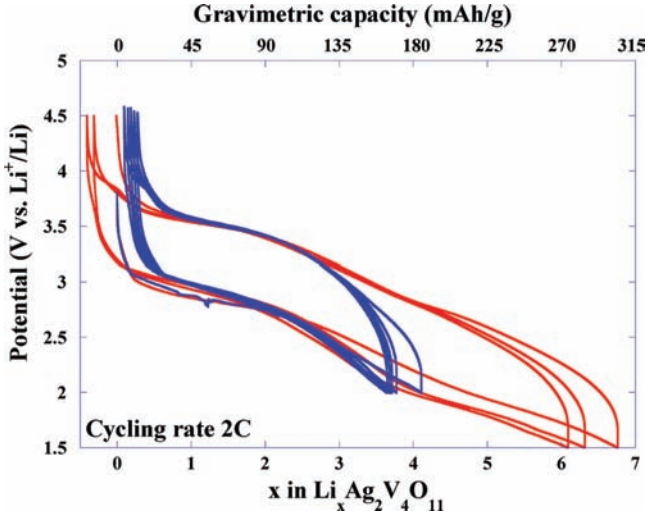

Figure 3. Galvanostatic curve recorded at 2C in the range 2−4.5 V or 1.5−4.5 V (vs Li^+/Li) of a composite SVO-RT/C_{sp} electrode in 1 M $LiPF_6$ EC/DMC 1:1 electrolyte.

used a 2C cycling rate that corresponds to the exchange of 2 lithium ions per hour. Note, for clarity reasons, we have used the empirical intercalation notation x in Li_x< host> description to refer to the amount of lithium in the host material (i.e., $Ag_2V_4O_{11}$). In comparison to the typical galvanostatic signature of SVO, two new features are revealed. At first, under similar cycling conditions, we observed the reduction potential of SVO_{nano} to be significantly higher than for microcrystalline SVO (see Supporting Information, Figure S2) and comes closer to the thermodynamic reduction potential of silver ion at 3.25 V.[25−27] The second aspect, from both a fundamental and an applied point of view, is the reversibility of the displacement reaction of silver by lithium ion, recognized in general, owing to the important ionic radii mismatch between Ag^+ and Li^+ ($r_{(Ag+)}$ = 1.15 Å vs $r_{(Li+)}$ = 0.76 Å),[30] to be poorly reversible.[24,28,29] The *in situ* XRD diffraction study performed during the insertion of lithium confirms the existence of a Li^+/Ag^+ displacement reaction on these nanocrystalline particles, as demonstrated by the appearance of two diffraction peaks at 2θ = 38.2° and 44.2°, corresponding to the (111) and (200) planes of metallic silver (Figure 4a). The displacement and then reduction of silver ion causes the collapse of the original crystal structure, in agreement with previous reports on microcrystalline SVO.[24,26,31,32] We have exploited the change in area of the Ag^0 (111) peak during the insertion of lithium under similar discharge regimes for two different sizes of acicular particles (Figure 4b). When nanosized SVO particles were used, we experienced the onset of the displacement reaction to take place earlier compared to microcrystalline SVO. This observation demonstrates a particle size dependence on the lithium insertion mechanism in SVO. Specifically, the release of silver metal progresses from $x = 0$ to $x \approx 3.0$ Li^+ inserted while the voltage discharge curve shows an S-shaped evolution, suggesting that the silver reduction competes with the V^{5+} reduction. This mechanism is in contrast to the previous study on microcrystalline SVO, for which it was reported that the reduction starts with a solid solution domain where V^{5+} is solely reduced before the silver is withdrawn from $x \approx 1$ Li^+ inserted.[22] This difference provides evidence that the competition between Ag^+

(25) Bergman, G. M.; Takeuchi, E. S. *J. Power Sources* **1989**, *26*, 365–367.
(26) Takeuchi, K. J.; Marschilok, A. C.; Davis, S. M.; Leising, R. A.; Takeuchi, E. S. *Coord. Chem. Rev.* **2001**, *219*, 283–310.
(27) Leifer, N. D.; Colon, A.; Martocci, K.; Greenbaum, S. G.; Alamger, F. M.; Reddy, T. B.; Gleason, N. R.; Leising, R. A.; Takeuchi, E. S. *J. Electrochem. Soc.* **2007**, *154*, A500–A506.
(28) Sauvage, F.; Bodenez, V.; Vezin, H.; Albrecht, T. A.; Tarascon, J.-M.; Poeppelmeier, K. R. *Inorg. Chem.* **2008**, *47*, 8464–8472.
(29) West, K.; Crespi, A. M. *J. Power Sources* **1995**, *54*, 334–337.
(30) Shannon, R. D. *Acta Crystallogr.* **1976**, *A32*, 751.
(31) Leising, R. A.; Thiebolt, W. C., III; Takeuchi, E. S. *Inorg. Chem.* **1994**, *33*, 5733–5740.
(32) Gleason, N. R. Palazzo, M. Leising, R. A., Takeuchi, E. S. Takeuchi, K. J. *208th ECS Meeting*, Los Angeles, CA, 2005, Abstract #248.

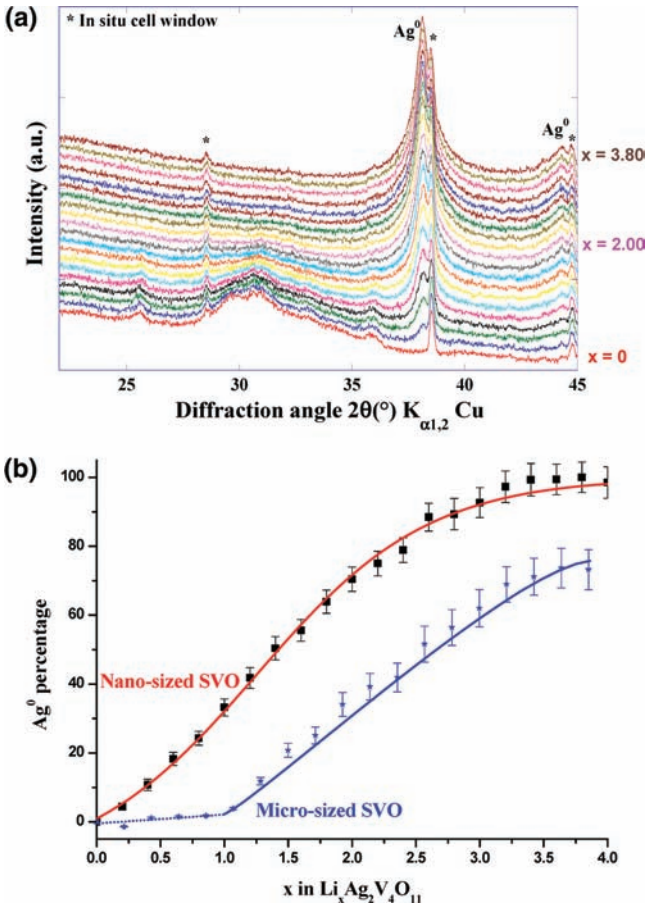

Figure 4. (a) *In situ* evolution of the XRD pattern for the lithium insertion in SVO-RT recorded at a D/10 discharge rate. (b) Comparison between the evolution of the silver metal peak area as a function of x in nanocrystalline and microcrystalline $Ag_2V_4O_{11}$.

and V^{5+} reduction is governed by two parameters, the size of the particle and the discharge rate, as discussed previously.[24]

This dependence can be rationalized by means of two different reduction paths driven by two distinct overpotential values (η) related either to the conventional lithium insertion mechanism or to the displacement reaction that involves the additional contribution of a particularly hindered process associated with the transport of Ag^+ within the framework. Reducing the particles leads therefore to a significant reduction in the diffusion length for the silver to withdraw from the core to the shell of the particle and consequently would alleviate noticeably the ohmic drop related to the displacement of silver ions. The case of SVOF is a good illustration of the benefit gained by reducing the particle size, as we experienced a decrease of 300 mV overpotential for the displacement of silver ions by reducing the particle size from 10 to 1 μm.[21] Interestingly, the well-established irreversible silver displacement reaction now becomes reversible for over 30 cycles, even under the high regime of 2C, as shown by the essentially constant capacity when cycling the cell between 3.8 and 2.3 V (Figure 5).

With the combination of the silver displacement reaction and V^{5+}/V^{3+} redox activity, the gravimetric capacity can be enhanced to more than 300 mAh/g for several cycles before the capacity declines owing to a lack of reversibility in the V^{5+}/V^{3+} redox couple. The result of the influence of cycling regime on the discharge capacity indicates that the room-temperature tailored

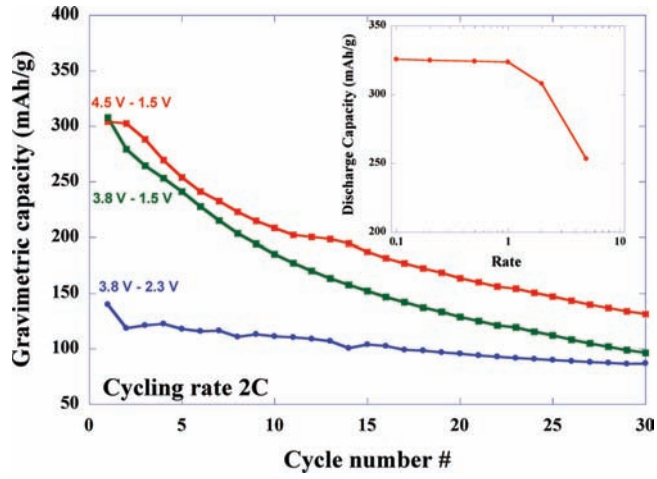

Figure 5. Capacity retention recorded on composite SVO-RT/C_{sp} electrode at 2C condition for different cycling potential windows. The influence of the cycling rate on the electrode capacity from 5C to C/10 is shown in the inset.

SVO particles are able to provide initial gravimetric capacity as high as 320−325 mAh/g at regimes below C, 305 mAh/g at 2C, and finally 252 mAh/g at 5C (Figure 5 inset). These values represent almost twice the gravimetric capacity of benchmark cathode materials, such as $LiCoO_2$, $LiFePO_4$, or $LiMnPO_4$. In comparison to the these materials, however, which have reached optimum performance, improved capacity retention remains to be accomplished to make the V^{5+}/V^{3+} redox couple more efficient. It is also noteworthy to mention that the electrochemical dissolution of the reoxidized Ag^+ in the electrolyte has not been experienced. This is further evidence of the effective reinsertion into the structure in its ionic form. The inset in Figure 5 shows how the discharge capacity down to 1.5 V is influenced by the cycling regime. We found that a gravimetric capacity as high as 325 mAh/g can be preserved as long as the regime does not exceed the C rate. Then it declines to 305 mAh/g at 2C and 254 mAh/g at 5C. Note that whatever the cycling rate, the capacity retention follows a similar pattern.

Conclusion

In conclusion, on the basis of our previous research demonstrating the synthesis under room-temperature control of $Ag_4V_2O_6F_2$ and $Ag_3VO_2F_4$, we have pursued the study of the ternary system $Ag_2O-V_2O_5-H_2O$ at a fixed ratio of HF (30). At this ratio the silver and fluoride content in the precipitate can be modified by the precursor concentration. In particular, the ternary system shows the existence of an unknown phase along with $Ag_4V_2O_6F_2$, $Ag_3VO_2F_4$, α-Ag_3VO_4, $Ag_4V_2O_7$, and α-$AgVO_3$. Adjustment of the reaction time and precursor concentration has enabled the synthesis of $Ag_2V_4O_{11}$ with an acicular morphology and size of $10-15 \times 50-200$ nm. We have demonstrated a new benefit of downsizing arising from the greater reversibility of the silver displacement reaction even under severe cycling regimes. As a result, the combination of two redox processes enables crossing the threshold of 1 e^-/formula unit for a cathode material and consequently boosting the gravimetric capacity over 300 mAh/g at 2C. This significant step forward paves the way to scrutinize further room-temperature chemistry in HF and also strongly encourages a new screening of silver-based transition metal oxide/oxyfluoride materials in their nanosized form for higher cathode performance in energy storage devices. Finally, this work is a step toward

greener chemistry with energy savings for chemical transformation while using types of solvent other than HF, which is one of our focuses.

Experimental Section

Nanosized $Ag_2V_4O_{11}$ (SVO-RT) was synthesized at room temperature using a 1/1.7 molar ratio of Ag_2O/V_2O_5 in an aqueous $HF_{(aq)}$ solution. Typically, 0.3972 g of Ag_2O and 0.5300 g of V_2O_5 were loaded in ambient air into a HF-resistant FEP-Teflon pouch containing 1.5 g of DI water and 0.88 g of $HF_{(aq)}$ (concentrated at 48−50% HF by weight). The pouches were then sealed, and the solution was allowed to react for 3 weeks at room temperature within the pouch in ambient air. The precipitate was then filtered to recover the nanocrystalline SVO particles.

α-Ag_3VO_4 was synthesized at room temperature from a 8/1 molar ratio of Ag_2O/V_2O_5 in an aqueous $HF_{(aq)}$ solution. Typically, 0.795 g of Ag_2O and 0.079 g of V_2O_5 were loaded in ambient air into a HF-resistant FEP-Teflon pouch containing 1.526 g of DI water and 0.281 g of $HF_{(aq)}$. The product was retrieved by vacuum filtration after 24 h reaction in the sealed Teflon pouches.

A similar procedure was used for the synthesis of $Ag_4V_2O_7$ and α-$AgVO_3$. For the first, a 6/1 molar ratio of Ag_2O/V_2O_5 corresponding to 0.696 g of Ag_2O and 0.079 g of V_2O_5 was incorporated in 20.0 g of DI water and 0.278 g of $HF_{(aq)}$. For the second, a 3/1 molar ratio of Ag_2O/V_2O_5 was incorporated in 6.01 g of DI water and 0.279 g of $HF_{(aq)}$.

Synthesis of $Ag_3VO_2F_4$ and $Ag_4V_2O_6F_2$ is similar to the one reported in ref 21.

The X-ray diffraction (XRD) patterns were recorded in a $\theta/2\theta$ configuration using a Bruker D8 diffractometer with Cu Kα radiation ($\lambda = 0.15418$ nm). The particle size and morphology were investigated either using an FEI Quanta 200FEG environmental scanning electron microscopy (ESEM) coupled with an energy dispersion spectroscopy (EDS) analysis system (Oxford Link Isis) or by HRTEM using a 200 kV FEI TECHNAI F20 S-TWIN microscope. Prior to observation, the sample was dispersed in ultrapure acetone before being deposited on a copper grid coated with a lacey-carbon film.

In situ XRD experiments were performed on a Bruker D8 diffractometer using a homemade electrochemical cell capped by a beryllium window functioning as the positive current collector.

The electrochemical characterization of SVO-RT was carried out by thoroughly manually mixing the particles with a 14 wt % amount of SP-type carbon black. The measurements were recorded in a two-electrode configuration using a Swagelok-type cell assembled in an Ar-filled glovebox. A lithium metal foil was then used as the counter and reference electrodes. Two pieces of Whatman GF/D borosilicate glass fiber sheets separator were thoroughly soaked with 1 M $LiPF_6$ EC/DMC 1:1 electrolyte (named LP30, Merck Selectipur grade). The electrode cycling tests were monitored by a VMP multipotentiostat (Biologic SA, Claix, France).

Acknowledgment. This work was supported from the Office of Naval Research (MURI Grant N00014-07-1-0620) and the National Science Foundation (Solid State Chemistry Awards No. DMR-0604454) and made use of the J. B. Cohen X-ray Facility supported by the MRSEC program of the National Science Foundation (DMR-0520513) at the Materials Research Center of Northwestern University. The authors wish to thank Dr. Thomas A. Albrecht for fruitful discussions.

Supporting Information Available: Full-pattern matching refinement of the X-ray diffraction patterns of (a) α-$AgVO_3$, (b) $Ag_4V_2O_7$, (c) α -Ag_3VO_4, (d) $Ag_4V_2O_6F_2$, and (e) $Ag_3VO_2F_4$ synthesized at room temperature. Note the background is caused by silicon glue used for the sample analysis. The evolution of the galvanostatic discharge curve recorded on SVO particles exhibiting different BET surface area from <1 to 28 m^2/g is also presented. This information is available free of charge via the Internet at http://pubs.acs.org.

JA1009713